

## Resistive switching of VO<sub>2</sub> films grown on a thermal insulator

Carl Willem Rischau<sup>1,\*</sup>, Stefano Gariglio<sup>1</sup>, Jean-Marc Triscone,<sup>1</sup> and Javier del Valle<sup>2,†</sup>

<sup>1</sup>Department of Quantum Matter Physics, University of Geneva, 24 Quai Ernest-Ansermet, 1211 Geneva, Switzerland

<sup>2</sup>Department of Physics, University of Oviedo, C/Federico Garcia Lorca 18, 33007 Oviedo, Spain

(Received 28 November 2023; revised 23 April 2024; accepted 11 June 2024; published 10 July 2024)

Many correlated oxides feature an insulator-to-metal transition as the temperature is increased. In thin films, this transition can be electrically induced by localized Joule heating, resulting in volatile resistive switching. Considering the importance of thermal effects, the thermal conductivity of the underlying substrate is expected to play a key role. Despite this, its influence has not been experimentally explored. Here, we compare the resistive switching of VO<sub>2</sub> films grown on two substrates with very different thermal conductivities  $k$ : sapphire [ $k \sim 50$  W/(m K)] and mica [ $k \sim 0.5$  W/(m K)]. While the overall features of the electrical switching are similar, the VO<sub>2</sub>-mica devices need around one order of magnitude less power to be switched, and their switching time is shorter. This can be understood by the improved thermal insulation offered by the substrate, which keeps the heat within the film. Our work shows that thermal insulators, such as mica, are a promising platform for energy-efficient volatile resistive switching.

DOI: 10.1103/PhysRevApplied.22.014021

### I. INTRODUCTION

Many transition metal oxides display an insulator-to-metal transition (IMT) as the temperature is increased [1,2]. This transition can be induced electrically by applying a sufficiently high voltage or current. Joule heating can trigger a local IMT, leading to the formation of a percolating metallic filament and a sharp drop in resistance [3–10]. The formation of this conducting filament does not result from the migration of ions, as in resistive memory devices, but from a locally induced insulator-to-metal transition triggered by current-generated Joule heating. Once the external voltage is removed, the filament cools and returns to the insulating state, yielding volatile resistive switching [11,12]. This phenomenon has attracted much attention in recent years, as it has been suggested as a viable option for a number of applications in information technologies, including optoelectronic switches [13–15], spiking neurons [16–25], and probabilistic bits [26,27].

In recent years, extensive work has been undertaken to understand what determines the switching properties in these materials, i.e., the sharpness ( $|\partial V/\partial I|$ ) of the voltage versus current ( $V$ – $I$ ) curve, the switching time, and the filament size. It has been suggested that the resistivity ratio across the transition,  $\rho_{ins}/\rho_{met}$ , could govern many of these properties [28–30]. The resistivity ratio broadly varies from compound to compound, taking values ranging from over  $10^5$ – $10^6$  for V<sub>2</sub>O<sub>3</sub> and  $10^3$ – $10^4$  for VO<sub>2</sub> and

NdNiO<sub>3</sub> to  $10$ – $10^2$  for Ti<sub>2</sub>O<sub>3</sub>, V<sub>3</sub>O<sub>5</sub>, and SmNiO<sub>3</sub> [1,2]. A large  $\rho_{ins}/\rho_{met}$  leads to a current focusing effect that results in sharper  $V$ – $I$  curves and faster switching since it sets the resistivities inside and outside the filament [28–30]. High resistivity ratios  $\rho_{ins}/\rho_{met}$  will confine the electric current to the region of the metallic filament and reduce Joule heating outside. Therefore, insulating areas stay cold and the filament is confined. For smaller resistivity ratios  $\rho_{ins}/\rho_{met}$ , the insulating area around the filament becomes leaky, leading to a current flow and an eventual broadening of the filament. Sharper  $V$ – $I$  curves and faster switching for larger  $\rho_{ins}/\rho_{met}$  is observed in the vanadate [28] and rare earth nickelate [29,30] families. For instance, switching in NdNiO<sub>3</sub> is fast ( $\sim 5$ – $500$  ns) and the associated  $V$ – $I$  curves are sharp, i.e., they have large discontinuities. Meanwhile,  $V$ – $I$  curves are smooth and continuous in SmNiO<sub>3</sub>, and switching times are one to two orders of magnitude slower. Nevertheless, it has also been suggested that the differences in substrate thermal conductivity can also explain these trends [29,31]. A substrate with large thermal conductivity would be more efficient at keeping insulating areas cooler and, therefore, more resistive. This, in turn, could lead to current focusing and sharper switching. As a result, this would mean that films grown on a low thermal conductivity substrate would inherently feature smooth  $V$ – $I$  curves and slow switching. On the other hand, it could be argued that a thermally insulating substrate would be more efficient at keeping heat on the film, accelerating the switching process and inducing sharp switching.

To investigate the effect of thermal conductivity, we have fabricated VO<sub>2</sub> microdevices on top of two substrates

\*Contact author: willem.rischau@unige.ch

†Contact author: javier.delvalle@uniovi.es

with a vast difference in thermal conductivity: sapphire ( $k \sim 50$  W/m·K) and mica ( $k \sim 0.5$  W/m·K). The change of  $\text{VO}_2$  resistance across the IMT is within the same order of magnitude. We observe that the shape of the  $V$ - $I$  curves is similarly sharp in both cases, with clear discontinuities. For comparable voltages, switching speeds are comparable or slightly faster for the mica case. However, we do observe an important difference: switching power is drastically reduced by using a thermally insulating substrate. These results show that thermal insulators can provide energy efficient and fast volatile resistive switching. This could be of great interest for the development of low power consumption in neuromorphic hardware [32,33].

## II. SAMPLE FABRICATION

The  $\text{VO}_2$  films were grown on R-cut sapphire (dimensions  $10\text{ mm} \times 10\text{ mm} \times 500\text{ }\mu\text{m}$  and mass  $\sim 180\text{ mg}$ ) and mica substrates ( $10\text{ mm} \times 10\text{ mm} \times 50\text{ }\mu\text{m}$  and  $\sim 17\text{ mg}$ ) via reactive sputtering from a  $\text{V}_2\text{O}_3$  target. The growth was performed with an Ar-O<sub>2</sub> gas mixture (2.8% O<sub>2</sub>) at a pressure of 4.3 mTorr at a temperature of 450 °C and the samples were cooled to room temperature at a rate of 10 °C/min. The thickness of the sputtered films was measured as 120 nm with a surface profiler. Raman measurements showed the growth of only one single phase in the films identical to that previously observed on single crystalline  $\text{VO}_2$  [34,35] (see Supplemental Material [36]). The sapphire substrates were manufactured by MTI Corp, with a reported out-of-plane thermal conductivity of  $k = 46.06$  W/m·K at 0 °C. The thermal conductivity of sapphire is weakly anisotropic, with the ratio between the out-of-plane and in-plane thermal conductivities amounting to around  $\sim 1.07$  [37]. High-quality muscovite mica substrates of grade V1 were obtained from Ted Pella Inc. with thermal conductivities at 0 °C of  $k = 0.54$  and 4 W/(m K) perpendicular and parallel to the cleavage planes, respectively [38,39]. To study resistive switching, an array of Au electrodes was patterned on the surface of the films using optical lithography (inset Fig. 1), leaving a 6.6 μm spacing between electrodes. The samples were measured inside a probe station that allowed for measurements up to 380 K, for which the sample was glued with thermally conductive copper tape to the heating stage. While mica presents a highly anisotropic thermal conductivity, its in-plane conductivity is still an order of magnitude smaller than that of sapphire.

## III. RESULTS AND DISCUSSION

Figure 1 shows the resistance of  $\text{VO}_2$  films grown on sapphire and mica as a function of temperature. For both substrates, the  $\text{VO}_2$  films display an IMT at  $\sim 340$  K with a change in resistance of 2–3 orders of magnitude. Although the transitions are quite similar for samples grown on the two substrates, there are small differences in the film

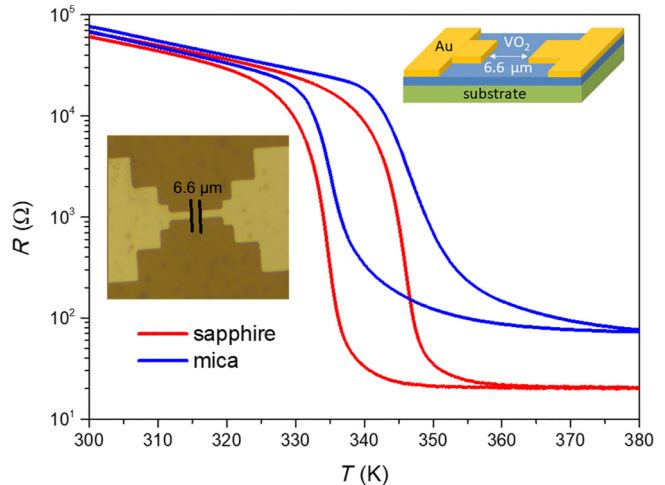


FIG. 1. Resistance  $R$  of  $\text{VO}_2$  films grown on sapphire and mica as a function of temperature  $T$ . The insets show a schematic view of the device with Au electrodes patterned at a distance of 6.6 μm as well as a microscopic image of the device.

resistivities. The resistance of both films in the insulating state is comparable, but films grown on sapphire have a lower metallic state resistivity and a slightly larger change across the IMT. The temperature-driven resistivity changes  $\rho_{ins}/\rho_{met}$  across the transition amount to  $\sim 3000$  and  $\sim 1000$  for sapphire and mica, respectively. The difference in resistivity change might be due to the different film orientations. Both films are polycrystalline, with a low degree of texture, visible in XRD scans (see Supplemental Material [36]). Films on sapphire substrates are textured along the [200]-direction. This direction is parallel to the vanadium chains and, therefore, is the one where film expansion and contraction are largest across the transition. This means that the [200]-texture-directed films can freely expand and contract along the IMT. Our  $\text{VO}_2$  films grown on mica, on the other hand, are textured along the [011]-direction, as also reported previously for mica substrates [40]. This means that the expansion and contraction are partially constrained in the plane, which results in strain developing across the IMT—as was shown for related compound  $\text{V}_2\text{O}_3$  [10]—that might explain the slightly lower change in resistivity for these samples.

Figures 2(a) and 2(b) show the direct current voltage versus current characteristics ( $V$ - $I$  loops) of the  $\text{VO}_2$  films grown on sapphire and mica substrates, respectively, measured by sweeping the current in steps of typically 0.1 mA. For both substrates, the  $V$ - $I$  curves show volatile resistive switching. At a threshold voltage  $V_{th}$ , the metallic filament percolates and the  $V$ - $I$  curves show a sharp and discontinuous jump that becomes sharper as the temperature is lowered. Above 340 K, the films are already metallic and no jumps are observed, as the voltage increases linearly with increasing current, following Ohm's law. It can be

noted that the VO<sub>2</sub> film grown on sapphire features extra switching discontinuities for an intermediate state at higher currents [see the gray-shaded area in Fig. 2(b)]. These are due to self-oscillations caused by the current source and the residual load resistance in series, which have been observed in numerous studies on resistive switching or memristors realized on various materials [10,17,29,41]. In this current range, the system is not stationary but oscillates between a state with a percolating filament and one without it. The presence of these device self-oscillations, however, does not modify the value of the switching power. The main difference between the two substrates is  $V_{th}$  and the corresponding threshold current  $I_{th}$  at which the volatile resistive switching occurs. Figure 2(c) compares the switching power  $P = V_{th}I_{th}$  as a function of temperature for the two different substrates. The switching power needed is around 5–10 times higher for sapphire than for mica.

The difference can be understood with a simple estimation of the heat flowing across a substrate of thickness  $d$ , area  $A$ , and a temperature difference of  $\Delta T$  across its two sides. The rate of heat flow is given by  $\dot{Q} = \kappa A \Delta T / d$ . The ratio of the rates of heat flow across the sapphire and the mica substrate is, thus, given by  $\dot{Q}_s/\dot{Q}_m = (\kappa_s/\kappa_m)(A_s/A_m)(\Delta T_s/\Delta T_m)(d_m/d_s)$ . With  $(\kappa_s/\kappa_m) \approx 100$ ,  $(A_s/A_m) \approx 1$ ,  $(d_m/d_s) \approx 0.1$ , and assuming  $(\Delta T_s/\Delta T_m) \approx 1$ , one obtains  $\dot{Q}_s/\dot{Q}_m \approx 10$ . Therefore, in the presence of the same temperature difference, the rate of heat flow will be around 10 times higher for the sapphire substrate compared with mica, which is in the same order of magnitude as the observed difference in switching power.

We also studied the time-dependent transport response of our devices upon application of a voltage pulse. A square voltage pulse of 2 ms was generated with a function generator and applied to one of the electrodes of the device. The other electrode of the device was connected to a  $50 \Omega$  impedance channel of an oscilloscope (see Supplemental Material [36]). Using this setup, we directly measured the electrical current passing through the device as a function of time. This is shown in Figs. 3(a) and 3(b) for both substrates ( $T = 335$  K). Several amplitudes of the voltage pulse are plotted in each case. At low voltages, i.e., 3 and 1.5 V for sapphire and mica, respectively, the IMT of VO<sub>2</sub> is not induced and the sample remains in the high resistance state. When a threshold voltage of 4 and 2 V is applied for mica and sapphire, respectively, the transition into the metallic state is triggered after some incubation time,  $\tau_{inc}$ , has passed. As shown in Fig. 3(c), the incubation time decreases as the applied voltage or the temperature is increased.

Comparing the sapphire and mica samples, we can see that the switching speed is comparable and only slightly faster for VO<sub>2</sub> grown on mica. Despite a large reduction in switching power, this similarity in switching speed can be understood by considering two competing effects. On

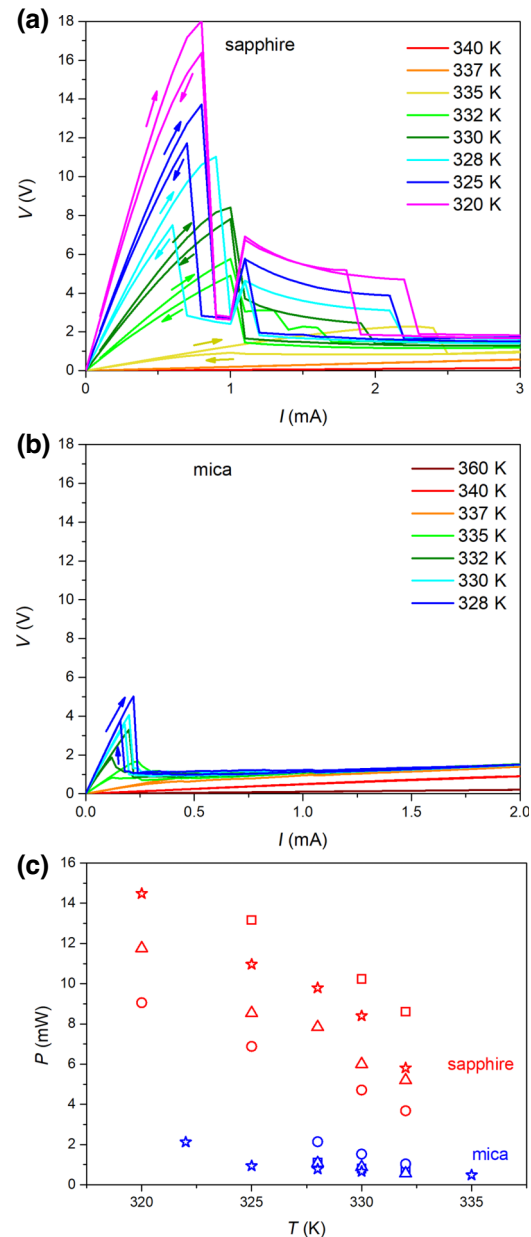


FIG. 2. Typical  $I$ – $V$  loops for devices on VO<sub>2</sub> films grown on (a) sapphire and (b) mica. Arrows indicate the sweeping direction of the current. The gray-shaded area in panel (a) marks the region where the device shows self-oscillations for temperatures 320, 325, 328, and 330 K. (c) Switching power  $P$  as a function of temperature  $T$  for several devices on sapphire (in red) and mica (in blue) substrates. Different symbols represent different devices.

one hand, the lower thermal conductivity of mica keeps the heat on the film, accelerating switching. On the other hand, a higher thermal conductivity reduces filament confinement and current focusing [31], reducing the positive feedback loop that leads to resistive switching and slowing the transition.

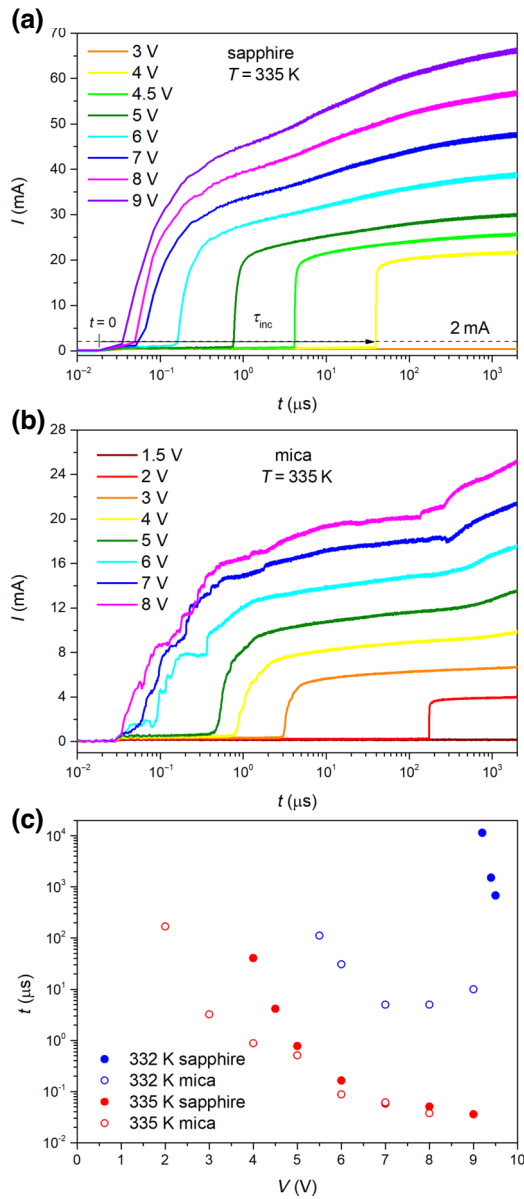


FIG. 3. Current versus time in  $\text{VO}_2$  devices grown on (a) sapphire and (b) mica substrates for IMTs triggered by different voltages at a temperature of 335 K. The incubation time  $\tau_{\text{inc}}$  indicated in panel (c) is the time between the application of the voltage pulse at  $t = 0$  s until the moment the IMT is triggered and a current of 2 mA is reached.

#### IV. CONCLUSIONS

In summary, we have fabricated two-terminal  $\text{VO}_2$  devices on sapphire and mica substrates, which have very different thermal conductivities. We observe that the sharpness of the resistive switching and the speed at which the device traverses from insulator to metal are comparable in both cases. However, we observe an order of magnitude decrease in the switching power. Our work shows that thermally insulating substrates are an excellent platform

for developing IMT-based neuromorphic hardware. Films grown on top of mica feature a volatile resistive switching that is as sharp and fast as those grown on sapphire, with the added benefit of lower power consumption.

#### ACKNOWLEDGMENTS

The authors thank Marco Lopes for his support during the fabrication and measurement of these samples. This work was funded by the U.S. Office of Naval Research through the NICOP Grant No. N62909-21-1-2028. Oxide growth was financed by the Swiss National Science Foundation through an Ambizione Fellowship (Grant No. PZ00P2\_185848). J.d.V. was funded by the Spanish Ministry of Science through a Ramón y Cajal Fellowship (Grant No. RYC2021-030952-I) and by Asturias FICYT under Grant No. AYUD/2021/51185 with the support of FEDER funds.

- [1] M. Imada, A. Fujimori, and Y. Tokura, Metal-insulator transitions, *Rev. Mod. Phys.* **70**, 1039 (1998).
- [2] S. Catalano, M. Gibert, J. Fowlie, J. Iñiguez, J. M. Triscone, and J. Kreisel, Rare-earth nickelates  $\text{RNiO}_3$ : Thin films and heterostructures, *Rep. Prog. Phys.* **81**, 046501 (2018).
- [3] G. Stefanovich, A. Pergament, and D. Stefanovich, Electrical switching and Mott transition in  $\text{VO}_2$ , *J. Phys.: Condens. Matter* **12**, 8837 (2000).
- [4] H. T. Kim, B. G. Chae, D. H. Youn, S. L. Maeng, G. Kim, K. Y. Kang, and Y. S. Lim, Mechanism and observation of Mott transition in  $\text{VO}_2$ -based two- and three-terminal devices, *New J. Phys.* **6**, 52 (2004).
- [5] Y. Zhou, X. Chen, C. Ko, Z. Yang, C. Mouli, and S. Ramanathan, Voltage-triggered ultrafast phase transition in vanadium dioxide switches, *IEEE Electron Device Lett.* **34**, 220 (2013).
- [6] A. Zimmers, L. Aigouy, M. Mortier, A. Sharoni, S. Wang, K. G. West, J. G. Ramirez, and I. K. Schuller, Role of thermal heating on the voltage induced insulator-metal transition in  $\text{VO}_2$ , *Phys. Rev. Lett.* **110**, 056601 (2013).
- [7] H. Madan, M. Jerry, A. Pogrebnyakov, T. Mayer, and S. Datta, Quantitative mapping of phase coexistence in Mott-Peierls insulator during electronic and thermally driven phase transition, *ACS Nano* **9**, 2009 (2015).
- [8] S. Kumar, M. D. Pickett, J. P. Strachan, G. Gibson, Y. Nishi, and R. S. Williams, Local temperature redistribution and structural transition during Joule-heating-driven conductance switching in  $\text{VO}_2$ , *Adv. Mater.* **25**, 6128 (2013).
- [9] P. Diener, E. Janod, B. Corraze, M. Querré, C. Adda, M. Guilloux-Viry, S. Cordier, A. Camjayi, M. Rozenberg, M. P. Besland, and L. Cario, How a dc electric field drives Mott insulators out of equilibrium, *Phys. Rev. Lett.* **121**, 016601 (2018).
- [10] S. K. Das, S. K. Nandi, C. V. Marquez, A. Rúa, M. Uenuma, E. Puyoo, S. K. Nath, D. Albertini, N. Baboux, T. Lu, Y. Liu, T. Haeger, R. Heiderhoff, T. Riedl, T. Ratcliff, and R. G. Elliman, Physical origin of negative differential resistance

- in V<sub>3</sub>O<sub>5</sub> and its application as a solid-state oscillator, *Adv. Mater.* **35**, 2208477 (2023).
- [11] J. del Valle, P. Salev, F. Tesler, N. M. Vargas, Y. Kalcheim, P. Wang, J. Trastoy, M. H. Lee, G. Kassabian, J. G. Ramírez, M. J. Rozenberg, and I. K. Schuller, Subthreshold firing in Mott nanodevices, *Nature* **569**, 388 (2019).
- [12] M. Samizadeh Nikoo, R. Soleiman-zadeh, A. Krammer, G. Migliato Marega, Y. Park, J. Son, A. Schueler, A. Kis, P. J. W. Moll, and E. Matioli, Electrical control of glass-like dynamics in vanadium dioxide for data storage and processing, *Nat. Electron.* **5**, 596 (2022).
- [13] S. Cueff, J. John, Z. Zhang, J. Parra, J. Sun, R. Orobctchouk, S. Ramanathan, and P. Sanchis, VO<sub>2</sub> Nanophotonics, *APL Photonics* **5**, 110901 (2020).
- [14] I. Olivares, L. Sánchez, J. Parra, R. Larrea, A. Griol, M. Menghini, P. Homm, L.-W. Jang, B. van Bilzen, J. W. Seo, J.-P. Locquet, and P. Sanchis, Optical switching in hybrid VO<sub>2</sub>/Si waveguides thermally triggered by lateral microheaters, *Opt. Express* **26**, 326541 (2018).
- [15] D. Lee, J. Lee, K. Song, F. Xue, S. Y. Choi, Y. Ma, J. Podkaminer, D. Liu, S. C. Liu, B. Chung, W. Fan, S. J. Cho, W. Zhou, J. Lee, L. Q. Chen, S. H. Oh, Z. Ma, and C. B. Eom, Sharpened VO<sub>2</sub> phase transition via controlled release of epitaxial strain, *Nano Lett.* **17**, 5614 (2017).
- [16] M. D. Pickett, G. Medeiros-Ribeiro, and R. S. Williams, A scalable neuristor built with Mott memristors, *Nat. Mater.* **12**, 114 (2013).
- [17] S. Kumar, J. P. Strachan, and R. S. Williams, Chaotic dynamics in nanoscale NbO<sub>2</sub> Mott memristors for analogue computing, *Nature* **548**, 318 (2017).
- [18] S. Kumar, R. S. Williams, and Z. Wang, Third-order nanocircuit elements for neuromorphic engineering, *Nature* **585**, 518 (2020).
- [19] J. del Valle, P. Salev, Y. Kalcheim, and I. K. Schuller, A caloritronics-based Mott neuristor, *Sci. Rep.* **10**, 1 (2020).
- [20] P. Stolar, J. Tranchant, B. Corraze, E. Janod, M.-P. P. Besland, F. Tesler, M. Rozenberg, and L. Cario, A leaky-integrate-and-fire neuron analog realized with a Mott insulator, *Adv. Funct. Mater.* **27**, 1604740 (2017).
- [21] M. Ignatov, M. Ziegler, M. Hansen, A. Petru, and H. Kohlstedt, A memristive spiking neuron with firing rate coding, *Front. Neurosci.* **9**, 376 (2015).
- [22] W. Yi, K. K. Tsang, S. K. Lam, X. Bai, J. A. Crowell, and E. A. Flores, Biological plausibility and stochasticity in scalable VO<sub>2</sub> active memristor neurons, *Nat. Commun.* **9**, 4661 (2018).
- [23] S. M. Bohaichuk, S. Kumar, G. Pitner, C. J. McClellan, J. Jeong, M. G. Samant, H. S. P. Wong, S. S. P. Parkin, R. S. Williams, and E. Pop, Fast spiking of a Mott VO<sub>2</sub>-carbon nanotube composite device, *Nano Lett.* **19**, 6751 (2019).
- [24] H. Lin and Y. Shen, A VO<sub>2</sub> neuristor based on microstrip line coupling, *Micromachines* **14**, 337 (2023).
- [25] P. Schofield, A. Bradicich, R. M. Gurrola, Y. Zhang, T. D. Brown, M. Pharr, P. J. Shamberger, and S. Banerjee, Harnessing the metal–insulator transition of VO<sub>2</sub> in neuromorphic computing, *Adv. Mater.* **35**, 2205294 (2023).
- [26] J. Del Valle, P. Salev, S. Gariglio, Y. Kalcheim, I. K. Schuller, and J.-M. Triscone, Generation of tunable stochastic sequences using the insulator-metal transition, *Nano Lett.* **22**, 1251 (2022).
- [27] T. J. Park, K. Selcuk, H. T. Zhang, S. Manna, R. Batra, Q. Wang, H. Yu, N. A. Aadit, S. K. R. S. Sankaranarayanan, H. Zhou, K. Y. Camsari, and S. Ramanathan, Efficient probabilistic computing with stochastic perovskite nickelates, *Nano Lett.* **22**, 8654 (2022).
- [28] J. del Valle, N. M. Vargas, R. Rocco, P. Salev, Y. Kalcheim, P. N. Lapa, C. Adda, M.-H. Lee, P. Y. Wang, L. Fratino, M. J. Rozenberg, and I. K. Schuller, Spatiotemporal characterization of the field-induced insulator-to-metal transition, *Science* **373**, 907 (2021).
- [29] T. Luibrand, A. Bercher, R. Rocco, F. Tahouni-Bonab, L. Varbaro, C. W. Rischau, C. Domínguez, Y. Zhou, W. Luo, S. Bag, L. Fratino, R. Kleiner, S. Gariglio, D. Koelle, J. M. Triscone, M. J. Rozenberg, A. B. Kuzmenko, S. Guénon, and J. Del Valle, Characteristic length scales of the electrically induced insulator-to-metal transition, *Phys. Rev. Res.* **5**, 013108 (2023).
- [30] J. del Valle, R. Rocco, C. Domínguez, J. Fowlie, S. Gariglio, M. J. Rozenberg, and J.-M. Triscone, Dynamics of the electrically induced insulator-to-metal transition in rare-earth nickelates, *Phys. Rev. B* **104**, 165141 (2021).
- [31] R. Rocco, J. Del Valle, H. Navarro, P. Salev, I. K. Schuller, and M. Rozenberg, Exponential escape rate of filamentary incubation in Mott spiking neurons, *Phys. Rev. Appl.* **17**, 24028 (2022).
- [32] D. Liu, H. Yu, and Y. Chai, Low-power computing with neuromorphic engineering, *Adv. Intell. Syst.* **3**, 2000150 (2021).
- [33] F. Qin, Y. Zhang, H. W. Song, and S. Lee, Enhancing memristor fundamentals through instrumental characterization and understanding reliability issues, *Mater. Adv.* **4**, 1850 (2023).
- [34] C. W. Rischau, X. He, G. Mazza, S. Gariglio, J.-M. Triscone, P. Ghosez, and J. del Valle, Oxygen isotope effect in VO<sub>2</sub>, *Phys. Rev. B* **107**, 115139 (2023).
- [35] E. R. Dobrovinskaya, L. A. Lytvynov, and V. Pishchik, *Application of Sapphire*, in: *Sapphire* (Springer, New York, NY, 2009), pp. 55–153.
- [36] See Supplemental Material at <http://link.aps.org/supplemental/10.1103/PhysRevApplied.22.014021> for details on the film characterization by XRD and Raman measurements, as well as the setup for the electrical measurements.
- [37] Manufacturing information from Ted Pella <https://www.tedpella.com>
- [38] A. S. Gray and C. Uher, Thermal conductivity of mica at low temperatures, *J. Mater. Sci.* **12**, 959 (1977).
- [39] W. Ren, W. Huang, H. Zhu, D. Wang, L.-G. Zhu, and Q. Shi, Flexible VO<sub>2</sub>/Mica thin films with excellent phase transition properties fabricated by RF magnetron sputtering, *Vacuum* **192**, 110407 (2021).
- [40] Y. Kalcheim, C. Adda, P. Salev, M.-H. Lee, N. Ghazikhani, N. M. Vargas, J. Del Valle, and I. K. Schuller, Structural manipulation of phase transitions by self-induced strain in geometrically confined thin films, *Adv. Funct. Mater.* **30**, 2005939 (2020).
- [41] T. D. Brown, S. M. Bohaichuk, M. Islam, S. Kumar, E. Pop, and R. S. Williams, Electro-thermal characterization of dynamical VO<sub>2</sub> memristors via local activity modeling, *Adv. Mater.* **35**, 2205451 (2023).